BIOENGINEERING

# Submilligram-scale separation of near-zigzag single-chirality carbon nanotubes by temperature controlling a binary surfactant system

**Dehua Yang[1,2], Linhai Li[1,2,3], Xiaojun Wei[1,2,4], Yanchun Wang[1,2], Weiya Zhou[1,2,4,5], Hiromichi Kataura[6], Sishen Xie[1,2,4,5], Huaping Liu[1,2,3,4,5]***



**Mass production of zigzag and near-zigzag single-wall carbon nanotubes (SWCNTs), whether by growth or separation, remains a challenge, which hinders the disclosure of their previously unknown property and practical applications. Here, we report a method to separate SWCNTs by chiral angle through temperature control of a binary surfactant system of sodium cholate (SC) and SDS in gel chromatography. Eleven types of single-chirality SWCNT species with chiral angle less than 20° were efficiently separated including multiple zigzag and near-zigzag species. Among them, (7, 3), (8, 3), (8, 4), (9, 1), (9, 2), (10, 2), and (11, 1), were produced on the submilligram scale. The spectral detection results indicate that lowering the temperature induced selective adsorption and reorganization of the SC/SDS cosurfactants on SWCNTs with different chiral angles, amplifying their interaction difference with gel. We believe that this work is an important step toward industrial separation of single-chirality zigzag and near-zigzag SWCNTs.**

## INTRODUCTION

The most valuable asset of single-wall carbon nanotubes (SWCNTs) for photonics applications is their structure-dependent optical transitions, which can be optically or electrically stimulated to emit light in the near-infrared (IR) wavelength range (*1*–*3*). This, together with the compatibility of SWCNTs with a range of biological (*4*), chemical (*5*), and complementary metal-oxide semiconductor processing methods (*6*, *7*), makes SWCNTs highly attractive for application as fluorescence markers in photoluminescence (PL) microscopy or as nanoscale emitters for on-chip data transmission with light (*8*–*10*). In particular, the $sp^3$ functionalization of SWCNTs enables not only tuning of their photon emission into telecom wavelengths but also great enhancement of their photon emission efficiency (*5*, *11*). The enhancement of the photoelectric properties of SWCNTs by $sp^3$ functionalization is heavily dependent on their chiral angle (*11*). As the chiral structures of SWCNTs move from near armchair to zigzag, $sp^3$ defect-state emission is progressively moved to the more red-shifted energy band, ultimately collapsing to emission from a single state in the true zigzag limit (*5*, *11*), implying that the nanotubes with smaller chiral angles may have previously unidentified and unique photoelectric properties. Industrial production of zigzag and near-zigzag single-chirality (*n*, *m*) species with identical properties is fundamental for the disclosure of their previously unknown properties and practical application in photonics, optoelectronics, and related integrated circuits.

In recent decades, intense efforts have been made to develop various methods, including synthetic methods (*12*–*15*) and separation techniques (*16*–*22*), for producing single-chirality SWCNTs and even their enantiomers, building a library of single-chirality species (*23*). Theoretical and experimental studies indicated that the growth rates of SWCNTs are directly proportional to their chiral angle (*24*–*27*). The selective growth of zigzag and near-zigzag SWCNTs remains difficult due to their low growth rate (*13*–*15*, *24*–*27*). Compared with growth methods, postgrowth separation techniques exhibit the advantages of simplicity, controllability, and scalability. Various separation techniques, such as aqueous two-phase extraction (ATPE) (*19*), density gradient centrifugation (DGU) (*20*), ion exchange chromatography (*21*), polymer wrapping (*22*), and gel chromatography (*8*, *16*–*18*), have been developed, achieving mass separation of several species such as (6, 4), (6, 5), (9, 4), and (10, 3) SWCNTs. Although it has been reported that zigzag and near-zigzag SWCNTs, including (9, 1) and (10, 0) SWCNTs, have been separated using DNA as a dispersant with the ATPE method (*19*), milligram-scale separation of these SWCNTs has not been achieved. One of the reasons may be the low content of these SWCNTs in the pristine SWCNT mixtures, given that the growth rates of near-armchair species are faster than those of zigzag and near-zigzag species (*13*–*15*, *24*–*27*). Another may be the low ability of the current separation techniques to recognize the chiral angle of SWCNTs, especially for zigzag and near-zigzag SWCNTs (*16*–*23*, *28*–*34*).

In the present work, we developed a method to realize submilligram-scale separation of near-zigzag single-chirality SWCNTs by temperature controlling their selective adsorption onto a gel medium in the binary surfactant system of sodium cholate (SC) and SDS. The gel chromatography technique has been demonstrated to be highly efficient, simple, and scalable (*8*, *16*–*18*). In this technique, the surfactants that disperse raw SWCNTs in an aqueous solution exhibit selective adsorption toward different-structure SWCNTs, producing a structural or coverage difference in the surfactant coating around different (*n*, *m*) SWCNTs (*16*–*18*), which induces their interaction difference with the gel medium and thus enables separation via their selective adsorption onto the gel. Recently, we demonstrated that SC exhibits adsorption selectivity toward the chiral angle of SWCNTs in the presence of SDS, while sodium deoxycholate (DOC) displays selectivity toward the diameter (*8*, *28*, *29*). However,

[1]Beijing National Laboratory for Condensed Matter Physics, Institute of Physics, Chinese Academy of Sciences, Beijing 100190, China. [2]Beijing Key Laboratory for Advanced Functional Materials and Structure Research, Beijing 100190, China. [3]Center of Materials Science and Optoelectronics Engineering, University of Chinese Academy of Sciences, Beijing 100049, China. [4]Songshan Lake Materials Laboratory, Dongguan, Guangdong 523808, China. [5]School of Physical Sciences, University of Chinese Academy of Sciences, Beijing 100049, China. [6]Nanomaterials Research Institute, National Institute of Advanced Industrial Science and Technology (AIST), Tsukuba 305-8565, Japan.
*Corresponding author. Email: liuhuaping@iphy.ac.cn

separation of SWCNTs by chiral angle has not been achieved with gel chromatography. In addition, pH (*30*, *31*), ethanol (*32*), strong salts (*33*), strong oxidants (*34*), and even temperature (*17*) have been proven to finely tune the surfactant coating by driving the selective adsorption onto different SWCNTs and to promote the separation efficiency of (*n*, *m*) SWCNTs because a slight difference of only 0.003% in the surfactant coating will produce very different interactions with gel (*8*, *28*, *29*). Among these techniques, temperature adjustment has the advantages of simplicity, efficiency, and being impurity free (*17*). On the basis of these results, we proposed combining temperature tuning and the binary surfactants SC and SDS to finely tune the selectivity of the surfactant coating toward the chiral angle of SWCNTs and thus realize high-efficiency separation of single-chirality SWCNTs with small chiral angles, especially zigzag and near-zigzag SWCNTs.

Here, we systematically investigate the effect of temperature on the selective adsorption of SWCNTs dispersed in a cosurfactant system of SC and SDS onto a gel column. The results show that only SWCNTs with chiral angles less than 20° were adsorbed in the gel column at temperatures less than 18°C. In contrast, at temperatures higher than 18°C, the SWCNTs with chiral angles larger than 20° start to adsorb in the gel column. On the basis of these results, we proposed two steps for the mass separation of zigzag and near-zigzag single-chirality SWCNTs. The first step is to separate the raw SWCNTs by diameter at the quasi-industrial scale at room temperature by using cosurfactants of SDS, SC, and DOC (*8*, *29*). Subsequently, by controlling temperature of the SDS and SC binary surfactants, SWCNTs with similar diameters are separated by chiral angle. The results show that we achieved nine types of single-chirality SWCNTs with chiral angle less than 20°, including (7, 3), (8, 3), (8, 4), (9, 1), (9, 2), (10, 2), (11, 0), (11, 1), and (12, 1) SWCNTs, accompanied by the separation of (6, 4), (6, 5), (7, 5), (7, 6), (9, 4), and (10, 3). Among them, more than 10 types of single-chirality species, including the near-zigzag species of (9, 1), (9, 2), (10, 2), and (11, 1), can be prepared on the submilligram scale in one-run separation, exhibiting potential for industrial preparation of near-zigzag single-chirality SWCNTs. These results indicate that temperature control is extremely important to enhance the selectivity of the gel to the chiral angles of SWCNTs in the binary surfactant system of SDS and SC. The submilligram separation of single-chirality SWCNTs with chiral angles less than 20° and even near-zigzag SWCNTs can be realized, which were difficult to separate in the past (*8*, *17*, *28*, *29*), let alone large scale. We further detected the structure of the SC/SDS surfactant layer on SWCNTs with different chiral angles and its evolution with the SDS/SC ratio and temperature using optical absorption spectra. Our present work lays a material foundation for fundamental property research and application of near-zigzag SWCNTs. The present technique also provides a reference for other methods, such as ATPE and DGU, for high-efficiency separation of zigzag and near-zigzag SWCNTs because the main feature of these techniques is that surfactants such as SDS and SC are used to distinguish the structure of various SWCNTs (*35*–*39*).

## RESULTS AND DISCUSSION

### Adsorption selectivity toward the chiral angle of SWCNTs

To reveal the effect of temperature on the selective adsorption of SWCNTs into a gel column in the binary surfactant system of SC and SDS, the separation temperature was varied to study the structure distribution of the SWCNTs adsorbed in the gel (see the detailed process in the experimental section). Raw high-pressure monoxide catalytically-grown SWCNTs (HiPco-SWCNTs) were dispersed in a binary surfactant solution of 0.5 weight % (wt %) SC and 0.5 wt % SDS. The initial separation temperature was set at 12°C, and 5 ml of an SWCNT dispersion was loaded into a 30-ml gel column. The unadsorbed SWCNTs were washed with an aqueous solution of 0.5 wt % SC and 0.5 wt % SDS, and the adsorbed SWCNTs were eluted by 5 wt % SDS. Subsequently, the unadsorbed SWCNTs were loaded into a second same gel column, whose temperature was increased by 2°C to separate the SWCNTs not adsorbed by the first gel column. In this manner, by increasing the separation temperature at a step of 2°C, the SWCNTs adsorbed at each temperature were collected. The separation schematic diagram is shown in Fig. 1A.

The SWCNTs separated at different temperatures were characterized and identified by their optical absorption spectra and PL contours (Fig. 1B and fig. S1) (*40*). The species adsorbed at different temperatures are summarized in Fig. 1C. Obviously, only SWCNTs with chiral angles of less than 20°, such as (7, 3), (8, 3), (8, 4), (9, 1), (9, 2), (9, 4), (10, 2), (10, 3), (11, 0), (11, 1), and (12, 1) species, were

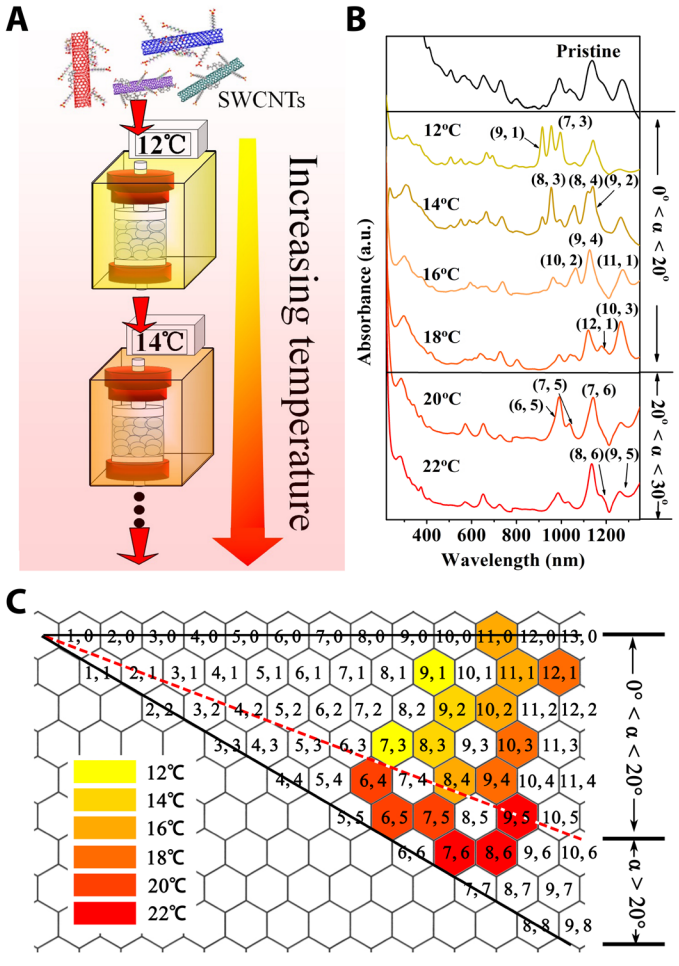


**Fig. 1. Temperature tuning the selective adsorption of SWCNTs by chiral angle.** (**A**) Schematic diagram of the separation of SWCNTs by chiral angle through temperature control. (**B**) Optical absorption spectra of the SWCNTs selectively adsorbed at various temperatures in the binary system of 0.5 wt % SC and 0.5 wt % SDS. a.u., arbitrary units. (**C**) Chirality map of the different chiral angle distributions of the SWCNTs selectively adsorbed at various temperatures.

adsorbed at 12° to 18°C. As the temperature increased from 12° to 18°C, a redshift of the first van Hove singularity transition absorption peak ($S_{11}$) was observed (Fig. 1B), indicating that the average diameter of the adsorbed SWCNTs increased, i.e., rough diameter separation of the nanotubes was simultaneously achieved. Note that the SWCNTs with large chiral angles, such as (6, 4) and (6, 5) near-armchair nanotubes, even if their diameters are small, could not be adsorbed at the low temperature of 12°C. With an increase in temperature to 18°C, trace amounts of small-diameter near-armchair SWCNTs were adsorbed. As the separation temperature increased to higher than 20°C, the near-armchair SWCNTs of (6, 4), (6, 5), (7, 5), (7, 6), and (8, 6) started to dominate in the adsorbed SWCNTs. These results demonstrate that lowering the separation temperature strongly enhanced the selectivity of the gel medium toward the chiral angle of SWCNTs in the binary surfactant system of SC and SDS, providing a simple method for high-efficiency separation of SWCNTs by chiral angle. A similar result has been observed when CoMoCAT (6, 5) SWCNTs (SG65i; Sigma-Aldrich), which are produced by Co-Mo catalysts, are used as raw materials (fig. S2), which suggests the generality of the present method.

## Submilligram-scale separation of single-chirality near-zigzag SWCNTs

It is well known that the atomic arrangement structure of a specific SWCNT is uniquely determined by its diameter and chiral angle. We expect that single chirality separation of zigzag and near-zigzag SWCNTs could be realized by successive separations by diameter and chiral angle, as shown in Fig. 2A. In the previous work, the surfactant DOC exhibits high recognition ability for the diameters of different SWCNTs (*8*, *29*). When the SWCNTs dispersed in the binary surfactants 1 wt % SDS and 0.5 wt % SC were loaded into a Sephacryl gel column, quasi-industrial diameter separation of the adsorbed SWCNTs could be obtained via stepwise elution by increasing the DOC concentration in the eluent (*8*, *29*). As shown in Fig. 2B, the optical absorption peaks of the eluted fractions by increasing DOC concentration show an overall redshift trend, suggesting that the diameter separation of SWCNTs was achieved, although the diameter separation shows some deviation possibly due to the presence of SC (*8*, *29*). The SWCNT fractions eluted at each DOC concentration exhibited a narrow diameter distribution but differed greatly in chiral angle. For example, the fraction eluted by 0.07 wt % DOC contained predominantly (6, 5) and (9, 1) SWCNTs with identical diameters and very different chiral angles. Single-chirality (9, 4) and (10, 3) SWCNTs were also achieved. Most of the separated fractions contained a higher content of the SWCNTs with chiral angles less than 20° than the raw materials, which provides feedstock suitable for single-chirality separation on a large scale.

Chiral angle separation was further performed at low temperatures, as shown in the right panel in Fig. 2A. The SWCNTs separated by diameter in the first step were simply redispersed in the binary surfactants SDS and SC and then loaded into a gel column at a low temperature (less than 18°C). In this manner, the SWCNTs with smaller chiral angles were adsorbed, while the species with larger chiral angles directly flowed through the gel column. Thus, high-efficiency separation of single-chirality SWCNTs with chiral angles less than 20° was obtained on a large scale. For instance, the SWCNT fraction containing (7, 3) and (6, 4) SWCNTs eluted at 0.06 wt % DOC was redispersed in the cosurfactants 0.5 wt % SC and 0.5 wt % SDS and then applied to a gel column at 15°C. The (7, 3) SWCNTs

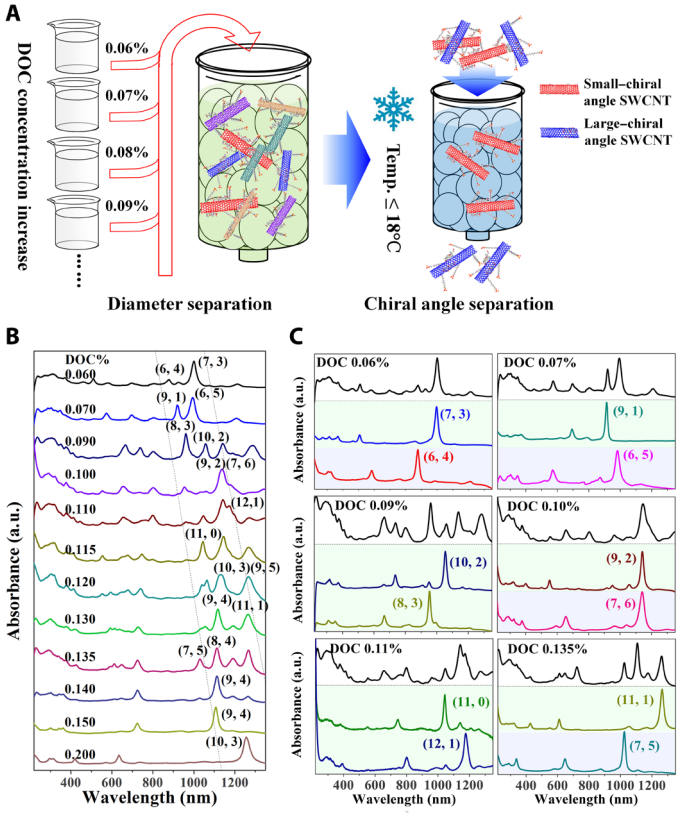


**Fig. 2. Separation of single-chirality zigzag and near-zigzag SWCNTs.** (**A**) Schematic diagram of the experimental scheme for separating single-chirality zigzag and near-zigzag SWCNTs through successive separations by diameter and chiral angle. (**B**) Optical absorption spectra of the SWCNTs separated by diameter at different DOC concentrations with fixed 0.5 wt % SC and 1.0 wt % SDS. (**C**) Optical absorption spectra of the nanotubes separated by chiral angle in the second step. In each spectral pattern, the top spectrum corresponds to one of the first separated SWCNT fractions eluted at different DOC concentrations, and the lower spectra are the optical absorption spectra of the corresponding second separated single-chirality fractions.

with a smaller chiral angle of 17° were adsorbed in the gel column, while the (6, 4) SWCNTs with a chiral angle of 23.41° directly flowed through the gel column. Thus, single-chirality (7, 3) SWCNTs were easily obtained, simultaneously accompanied by enrichment of (6, 4) SWCNTs in the flow-through dispersion, as shown in the top left panel in Fig. 2C.

Similar procedures were performed to separate other species (Fig. 2C and fig. S3). The concentration/ratio of SDS and SC was slightly adjusted to separate the small–chiral angle SWCNTs with larger diameters [for example, (9, 2), (10, 2), and (11, 1) SWCNTs]. Meanwhile, the separation temperature was higher for these species. The use of the different separation conditions will be discussed later. The experimental details of separating different species are shown in the experimental section and also in fig. S4. With this technique, nine single-chirality SWCNTs with chiral angle less than 20° including (7, 3), (8, 3), (8, 4), (9, 1), (9, 2), (10, 2), (11, 0), (11, 1), and (12, 1) were separated by a simple one-column flush procedure, which was difficult to achieve previously. The unadsorbed near-armchair SWCNTs of (6, 4), (6, 5), (7, 5), and (7, 6) were subsequently extracted from the flow-through fractions. Together with (10, 3) and (9, 4) SWCNTs in the first step, 15 single-chirality species were separated

(as shown in Fig. 3, A and B). Because of the simple separation process, submilligram-scale separation of single-chirality species of (7, 3), (7, 6), (8, 3), (8, 4), (9, 1), (9, 2), (10, 2), and (11, 1) was achieved (Fig. 3D) using a 200-ml gel column. The purity of the separated SWCNTs was evaluated with a previous method (*16*). PeakFit software was used to simulate the near-IR optical absorption spectra representing the individual (*n*, *m*) species with wavelengths from 700 to 1350 nm, as shown in fig. S5. The purity of each (*n*, *m*) species was computed as the ratio of the area of the dominant absorption peak to the sum of all peak areas in the near-IR region. The results are integrated in Fig. 3C. The purity of 10 species is greater than 90%, and only the purity of the (11, 0) species is below 80%, indicating that the present technique is highly efficient in recognizing the atomic structures of SWCNTs, especially for the SWCNTs with chiral angles less than 20°. Note that, although the stock SWCNT solution was dispersed for 5 hours at 0.38 W/ml before separation, high ratio of G-band/D-band in Raman spectra for different (*n*, *m*) species evidenced that the dispersion process did not introduce too many defects (fig. S6). When the dispersion time was reduced to 30 min, we demonstrated that high-purity single-chirality species could also be isolated and they have longer length and higher PL intensity. However, the concentration of the monodispersed SWCNT solution was greatly reduced, which would inevitably decrease the overall throughput of the separated species (fig. S7). Recently, by characterizing the PL spectra of the separated single-chirality SWCNTs, we revealed the relationship between the PL quantum yield and the chiral structure of SWCNTs (*41*).

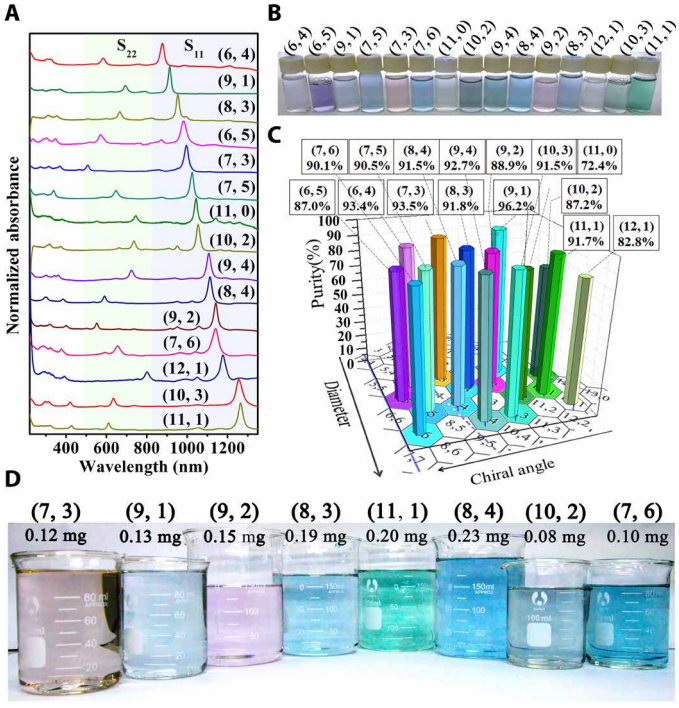


**Fig. 3. Characterization of the separated single-chirality species.** (**A**) Optical absorption spectra of 15 types of single-chirality species separated by the temperature control technique. (**B**) Photographs of the separated single-chirality SWCNTs. (**C**) Purity distribution of various single-chirality (*n*, *m*) species. (**D**) Solution photographs of the submilligram-scale single-chirality near-zigzag species. The mass of each (*n*, *m*) SWCNT was calculated on the basis of its optical absorbance at 280 nm (*60*). Photo credit: Dehua Yang, Institute of Physics, Chinese Academy of Sciences.

## Detecting the temperature-driven surfactant coating change

The length distribution of the separated (*n*, *m*) species is basically identical, ranging from 100 to 700 nm (fig. S8), indicating that length difference is not the main cause for the separation of zigzag and non-zigzag SWCNTs. Lowering the temperature would decrease the solubility of SDS and SC in the aqueous solution and facilitate their aggregation (*42*–*44*), driving their selective adsorption onto distinct (*n*, *m*) SWCNTs (*17*). Our abovementioned results indicate that the temperature-driven adsorption of surfactants onto SWCNTs should be chiral angle–dependent in the binary system of SDS and SC, which enlarges the difference in the surfactant coatings around SWCNTs with different chiral angles. The optical transition properties of SWCNTs are sensitive to the adsorbed molecules, including various surfactant molecules, because of changes in the molecular interaction with SWCNTs, dielectric environment, or strain effect around them (*17*, *45*–*49*). To detect the selective adsorption of the binary surfactants SDS and SC onto (*n*, *m*) species with different chiral angles driven by lowering the temperature, we explored the effect of temperature on the spectral changes in the first van Hove singularity transition ($S_{11}$) absorption peak of single-chirality (9, 1) and (6, 5) species with identical diameters but different chiral angles, which were highly dispersed in an aqueous solution of the cosurfactants 0.5 wt % SDS and 0.5 wt % SC. The results show that lowering the temperature induces a clear redshift and quenching of the $S_{11}$ optical absorption peak of both types of SWCNTs (Fig. 4). The $S_{11}$ peak of (6, 5) SWCNTs exhibits a greater redshift than that of (9, 1) SWCNTs, while the quenching degree is smaller. These results imply that more surfactant molecules should selectively adsorb onto (6, 5) SWCNTs and form a denser or tighter surfactant coating at lower temperatures, resulting in much weaker adsorbability onto gel. The more compact surfactant coating also protects the (6, 5) SWCNTs from oxidation and protonation by oxygen or hydronium ions in an aqueous solution such that the quenching degree is smaller than that of the (9, 1) SWCNTs (*49*). We can anticipate that three possible processes occur in the adsorption of the cosurfactants onto SWCNT surfaces driven by lowering the temperature: (i) the ratio of SC and SDS in the surfactant coating around a specific SWCNT remains unchanged or (ii) the composition ratio of the cosurfactants changes, and (iii) the morphology and structure of the cosurfactant coating changes via reorganization.

The physical adsorption of surfactants onto SWCNTs is a dynamic equilibrium phenomenon. The adsorption probability of each surfactant mainly depends on its concentration and ratio in the mixed surfactants (*16*, *17*). To verify the possibility of the first process occurring, we ideally assume that the composition ratio of the surfactant coating around an SWCNT remains constant as the concentration of each surfactant component in the solution increases equally. For this, we investigated the effect of the concentration of SDS and SC on the optical absorption spectral change while fixing their concentration ratio to 1:1, in which the concentration of each surfactant was simultaneously varied from 0.5 to 2 wt %. The results show that the wavelength of the $S_{11}$ peaks of both nanotubes remains unchanged (fig. S9 and Supplementary Materials) at a fixed temperature. These results are different from the results induced by lowering the temperature that we observed, indicating that lowering

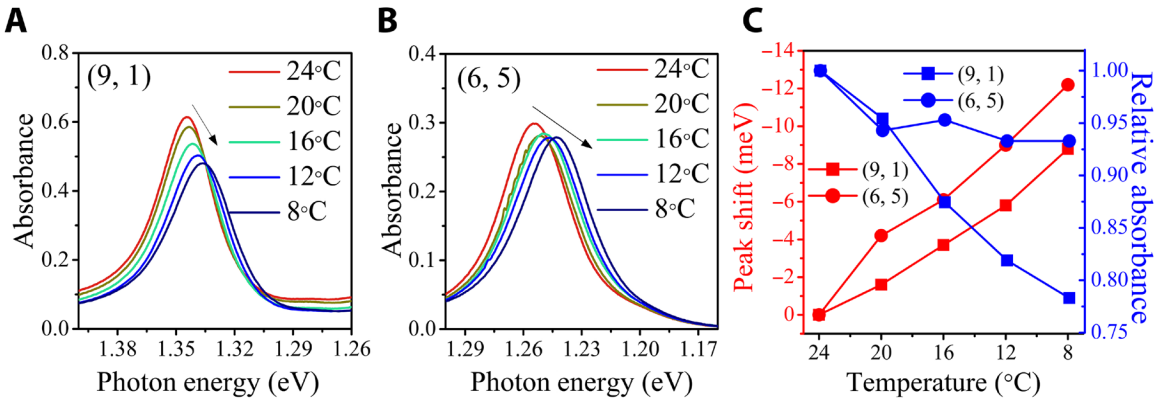


**Fig. 4. Temperature effect on the optical absorption spectra of the (6, 5) and (9, 1) SWCNTs.** (**A** and **B**) $S_{11}$ absorption peaks of (6, 5) and (9, 1) dispersed in 0.5 wt % SC and 0.5 wt % SDS at various temperatures. (**C**) Plots of redshift and relative absorbance of the $S_{11}$ peaks of (9, 1) and (6, 5) SWCNTs as a function of temperature.

the temperature does not simply increase the surfactant density around SWCNTs, and the ratio of SDS and SC adsorbed on SWCNTs is likely altered at lowered temperatures.

We further studied the spectral changes of (9, 1) and (6, 5) species by varying the concentration ratio of SDS and SC at different temperatures, which could drive a composition ratio change of the surfactant coating around SWCNTs. The results are presented in Fig. 5A and figs. S10 to S12. As the SDS concentration increases while fixing the SC concentration at 0.5 wt %, the shift of the $S_{11}$ absorption peaks of (6, 5) and (9, 1) SWCNTs shows similar changes at different temperatures. In general, the spectral changes can be divided into three stages. In the first stage, when the SDS concentration gradually increases from 0 to 0.5 wt %, the $S_{11}$ peaks of both the (9, 1) and (6, 5) nanotubes exhibit an increasing redshift, reaching a maximum at approximately 0.5 wt % SDS. In the second stage, when the SDS concentration increases from 0.5 to 1.0 wt %, the $S_{11}$ peak position fluctuates slightly. In the third stage, with an increase from 1.0 to 2.0 wt %, the $S_{11}$ peaks of the (9, 1) and (6, 5) blueshift are back. Similarly, when the SDS concentration is fixed at 2 wt %, the addition of SC to the SDS dispersing SWCNTs also causes a redshift of the $S_{11}$ peaks of (9, 1) and (6, 5) SWCNTs. In comparison, the redshift of the (6, 5) SWCNTs is substantially greater than that of the (9, 1) SWCNTs regardless of whether SDS is added to the SC dispersing SWCNTs or SC to the SDS dispersing SWCNTs. Note that the change in the surfactant composition ratio redshifts the $S_{11}$ absorbance of (6, 5) SWCNTs by 8 meV and (9, 1) SWCNTs by 3 meV at most at 24°C, which is smaller than the redshift caused by lowering the temperature from 24° to 8°C at the fixed concentrations of 0.5 wt % SDS and 0.5 wt % SC [13 meV for (6, 5) and 9 meV for (9, 1) SWCNTs]. On the basis of the above results, we believe that the spectral redshift induced by temperature reduction may be due, in part, to a change in the SDS/SC ratio on SWCNTs.

In the single-surfactant SDS system, a redshift of the optical absorption spectrum was also reported with lowering of the temperature (*17*). The spectral change was attributed to the change in the microdielectric environment or strain enhancement of SWCNTs due to the adsorption and reorganization of the surfactant (*17*, *45*–*48*). However, the redshifts caused by lowering the temperature from 24° to 8°C in the single-surfactant SDS or SC system are less than 5 meV for (9, 1) and (6, 5) SWCNTs (figs. S13 and S14), which is much smaller than that in the case of the mixed surfactants [13 meV for (6, 5) and 9 meV for (9, 1) SWCNTs] (Fig. 5A). In combination with the above results, whether adding SDS to the SC-dispersing SWCNTs or adding SC to the SDS-dispersing SWCNTs will cause marked redshift of optical absorption spectra, we propose that the interaction between SDS and SC should be present in the binary surfactant system because a simple competitive adsorption or replacement between SDS and SC on the surface of SWCNTs should not cause a large spectral redshift (*50*–*52*). Compared to the head-tail surfactant SDS, SC shows a lower self-aggregation tendency and allows tighter SC coating of the SWCNT surface by accommodating the SWCNT curvature and wrapping around the SWCNTs like a ring, preventing the adsorption of SWCNTs on gel (*53*), while SDS is prone to form a more loosely packed structure owing to van der Waals interactions on SWCNT surfaces (*54*, *55*), allowing for a stronger interaction of SWCNTs with the gel. Several studies have reported that the flexible alkyl chains of SDS tend to interact with the nonplanar hydrophobic β-faces of SC molecules to form compound micelles of SDS/SC (*56*–*59*). We propose that the introduced SDS molecules likely shift the dynamic equilibrium of the physisorption of SC molecules on SWCNTs and destroy the well-packed SC coating by removing a fraction of monomeric SC molecules on SWCNTs and forming SDS/SC compound (cosurfactant) that loosely coat the SWCNTs, leading to increase in the exposure area of SWCNT sidewalls (as shown in Fig. 5B), which enhances the adsorbabililty of SWCNTs onto gel. Compared with single surfactant SDS or SC dispersing (9, 1) and (6, 5) SWCNTs, the adsorption of SDS/SC compound on SWCNTs causes a great redshift of the $S_{11}$ optical absorption peak, probably due to the increase in the contact area and the enhancement of the interaction between SWCNTs and cosurfactants (Fig. 5A and fig. S14). Because of the presence of chiral SC molecules, the compound surfactants prefer to adsorb on the SWCNTs with larger chiral angles, resulting in a larger redshift of the $S_{11}$ peak of (6, 5) SWCNTs than (9, 1) SWCNTs. This hypothesis is consistent with the change trend of the optical absorbance of SWCNTs. With the introduction of SDS, the optical absorbance of SWCNTs decreases likely because the formation of the loosely SDS/SC layer weakens the protection of SWCNTs from oxidation. Because of the relatively dense SC/SDS layer, the absorbance of (6, 5) SWCNTs decreases less compared with (9, 1) species (fig. S12). It has been reported that dissolved oxygen may cause the spectral redshift of

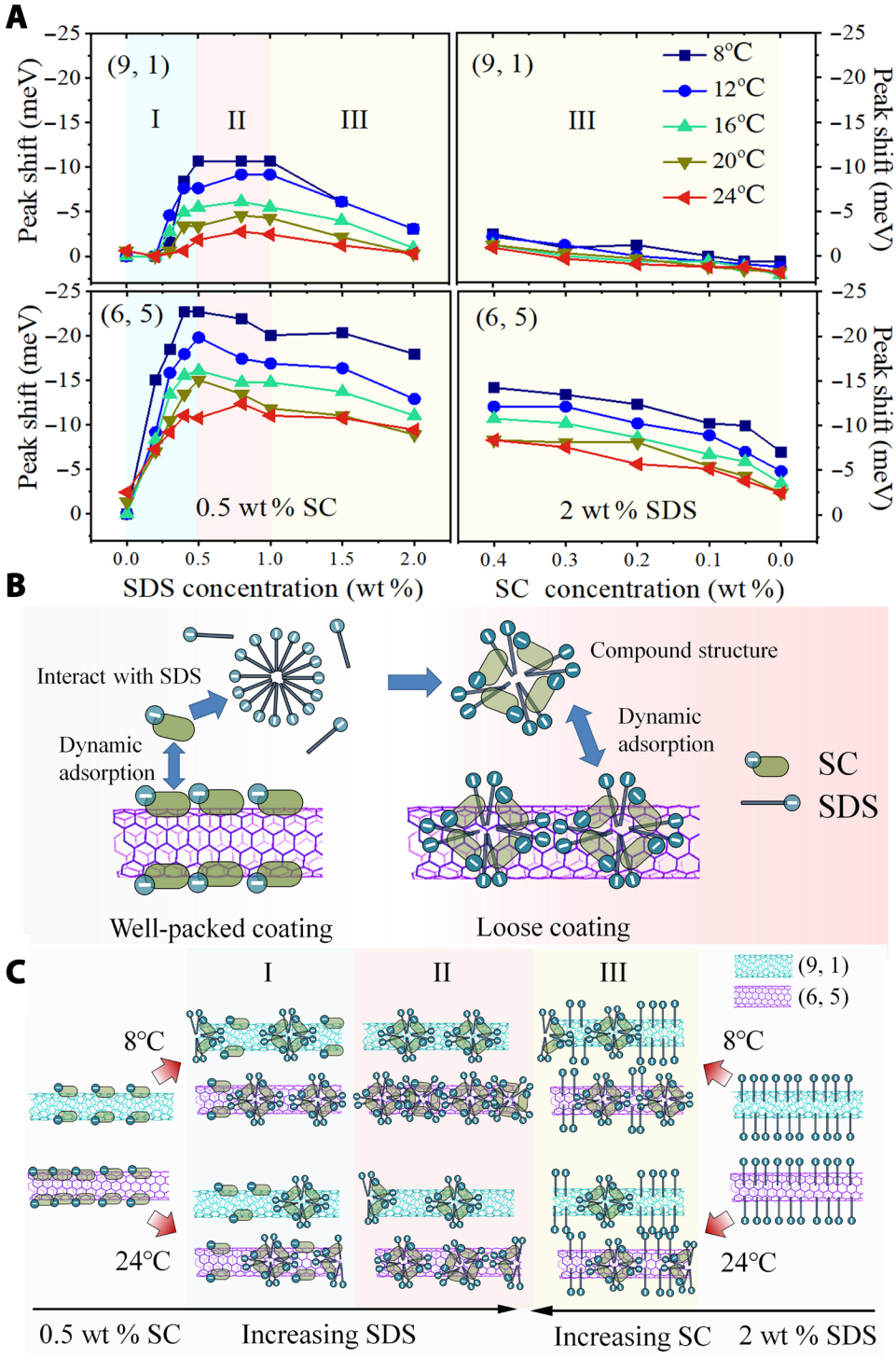


**Fig. 5. Effect of the SDS/SC concentration ratio and temperature on the $S_{11}$ peak shifts of (6, 5) and (9, 1) and the surfactant coating on them.** (**A**) $S_{11}$ peak shifts of (6, 5) and (9, 1) as a function of the concentration ratio of SC and SDS at various temperatures. Notably, the SDS concentration is varied with fixed 0.5 wt % SC in the left two panels; the SC concentration is varied with fixed 2 wt % SDS in the right two panels. (**B**) Schematic illustration of the surfactant coating structure change on an SWCNT when SDS molecules are introduced into SC dispersing SWCNTs. (**C**) Schematic illustration of the effect of the SDS/SC ratio on the surfactant coating change on SWCNTs. The colored regions correspond to the three stages in (A).

SWCNTs due to the reorganization of surfactant layer resulting from oxidation (*34*). Here, the dissolved oxygen may partially contribute to the spectral shift of SWCNTs due to the loosely SDS/SC coat.

The density of the SDS/SC cosurfactant adsorbed on SWCNTs should strongly depend on the concentrations and ratio of SC and SDS. As shown in Fig. 5C, with the introduction of SDS (less than that of SC) in the first stage, the SDS/SC cosurfactant starts to

form and adsorb on SWCNTs. However, because of the low SDS concentration, much of the surface area is still covered by well-packed SC, which results in weak adsorbability onto the gel. With an increase in the SDS concentration, an increasing amount of SDS/SC cosurfactant is formed. When the SDS concentration increases to 0.5 to 1.0 wt % (equal to that of SC or higher), the concentration of the SDS/SC cosurfactant reaches the maximum and dominates the surface coating on SWCNTs. The exposure area of the SWCNT sidewalls reaches the largest value. With a further increase in the SDS concentration, SDS molecules gradually replace the SDS/SC compound surfactant and lastly dominate the surfactant layer structure on SWCNTs, resulting in the $S_{11}$ peak shifting back to the blue region. In comparison, the relative blueshift of the $S_{11}$ peak of (6, 5) SWCNTs is significantly smaller than that of (9, 1) SWCNTs. For example, the $S_{11}$ peak of (6, 5) SWCNTs blueshifts back by ~24% of the maximum redshift at an SDS concentration of 2 wt %, while that of (9, 1) shifts back by ~88% of the previous redshift at 24°C possibly because the interaction between the SDS/SC cosurfactant and (6, 5) SWCNTs is stronger, making the cosurfactant more difficult to replace by monomeric SDS (*29*).

According to the experimental results and the proposed structure of the cosurfactant SDS/SC coating, we further put forward the structural change of the cosurfactant layer caused by the temperature decrease. At room temperature (24°C), although the coating structure of the cosurfactant was tuned by altering the concentration of SDS and SC, reaching the maximum redshift at 0.5% SDS/0.5% SC of 8 meV for (6, 5) and 3 meV for (9, 1), the difference in the coating is not sufficient to separate the SWCNTs by chiral angle. The selective adsorption onto gel by chiral angle can be observed only by overloading, but a large number of near-armchair SWCNTs are still adsorbed in the gel (fig. S15). Lowering the temperature induces a further spectral redshift of (6, 5) and (9, 1) SWCNTs at various ratios of SDS/SC (Fig. 5A), implying that more cosurfactants should adsorb and reorganize on the SWCNTs driven by the reduction in the solubility of surfactants (as shown in Fig. 5C) (*43*, *44*). Because of the different effects of temperature on the solubility of SDS and SC, the ratio of SDS/SC in the cosurfactant coating adsorbed on SWCNTS is likely altered at lowered temperatures (*42*, *56*). (6, 5) SWCNTs exhibit a greater redshifts than (9, 1) SWCNTs (Fig. 5A and table S1) at various concentrations of SC and SDS and smaller quenching in the $S_{11}$ peak (fig. S12). As shown in Figs. 5A and 4C, lowering the temperature from 24° to 12°C further induces a redshift of the $S_{11}$ peaks of (6, 5) by 9 meV and (9, 1) by 5.8 meV at 0.5 wt % SDS/0.5 wt % SC. These results indicate that a tighter or denser cosurfactant coating is selectively adsorbed on (6, 5) SWCNTs compared to (9, 1) SWCNTs, which further amplifies the interaction difference of (6, 5) and (9, 1) SWCNTs with the gel. Thus, the denser and tighter SDS/SC cosurfactant markedly weakens the adsorbability of (6, 5) SWCNTs onto the gel, while the adsorbability of (9, 1) SWCNTs is preserved at a lower temperature. Actually, it is a very complex and systematic task to fully illustrate the structure of the SC/SDS surfactant layer and how it varies with the SDS/SC ratio and temperature. In this work, we only proposed a possible model on the basis of spectral detection (Fig. 5). More systematic studies are needed to clarify the structure of SDS/SC cosurfactant layer and its evolution with environment.

### Effect of the ratio of SDS and SC on the adsorbability of SWCNTs

The hydrophobic interaction and electrostatic repulsion between SDS and SC molecules can be adjusted by changing the ratio and the total concentration of these two surfactants, which will tune the molecular self-assembly process on SWCNTs. The critical point for the structural separation of nanotubes via gel chromatography is the selective adsorption of SWCNTs into the gel medium, which strongly depends on the exposure area of the SWCNT sidewalls. As mentioned above, the separation of (9, 1) SWCNTs from a (6, 5)/(9, 1) mixture was achieved under 0.5 wt % SC and 0.5 wt % SDS because of the maximum difference in the cosurfactant coating at a low temperature. For the separation of larger-diameter SWCNTs, the concentration/ratio should be tuned for the same purpose. Given that the SC molecules need not bend to a great extent to cover an SWCNT with a larger radius, the larger-diameter SWCNTs should have a stronger interaction with SC molecules and usually form a denser SC coating (*59*). Thus, more SDS molecules should be introduced to interact with or replace SC adsorbed on SWCNTs to form the SDS/SC cosurfactant, increase the exposure area of the nanotube surface, and enable adsorption onto gel.

To verify the effect of the concentrations and composition ratio of the mixed surfactants on their selective adsorption onto SWCNTs at low temperatures, we further investigated the separation of SWCNTs based on their chiral angle by varying the surfactant concentration/ratio. In this experiment, we dispersed SWCNTs in 0.5 wt % SC and 0.3 wt % SDS, 0.5 wt % SC and 0.4 wt % SDS, 0.5 wt % SC and 1 wt % SDS, 0.05 wt % SC and 2 wt % SDS, and 0.5 wt % SC and 2 wt % SDS. In both cases of 0.5 wt % SC/0.3 wt % SDS and 0.5 wt % SC/2 wt % SDS, adsorption of SWCNTs onto the gel medium was not observed, possibly due to the well-packed surfactant coating around them. In the other cases, the nanotubes adsorbed at temperatures of 12° to 22°C were characterized by the optical absorption spectra (fig. S16), and the relative contents of different (*n*, *m*) species among the adsorbed SWCNTs are summarized in Fig. 6. In both cases of 0.4 wt % SDS/0.5 wt % SC and 1 wt % SDS/0.5 wt % SC, the SWCNTs with smaller chiral angles can selectively adsorb at low temperatures, showing strong chiral angle selectivity. The selective adsorption of small-diameter species with smaller chiral angles is even more distinct for the case of 0.4 wt % SDS/0.5 wt % SC, but the amount of adsorbed SWCNTs, especially large-diameter nanotubes, is much smaller (fig. S16). The (11, 1), (10, 2), (10, 3), and (9, 4) SWCNTs with relatively large diameters were not adsorbed. This should be attributed to the stronger interaction of SC molecules with these SWCNTs and thus the denser SC coating on them. Meanwhile, as we predicted, in the case of 0.5 wt % SC and 1 wt % SDS, where SDS is higher than SC in concentration, chiral angle selectivity still dominates, while the adsorbability of SWCNTs with relatively large diameters or medium chiral angles (slightly smaller than 20°) is enhanced. This scenario is consistent with the use of 0.5 wt % SC and 1 wt % SDS or 0.25 wt % SC and 1.25 wt % SDS for the separation of single-chirality (11, 1), (10, 2), (10, 3), and (9, 4) SWCNTs that have larger diameters. In the situation of 0.05 wt % SC and 2 wt % SDS, in which a trace amount of SC is introduced, chirality selectivity at low temperature (at 12°C) is also observed. As shown in Fig. 6A and fig. S16, a small amount of multiple (*n*, *m*) species with chiral angles less than 20° [i.e., (9, 1), (7, 3), and (8, 3) SWCNTs] is adsorbed in the gel column, indicating that chiral angle selectivity emerges. In contrast, only near-armchair nanotubes, such as (6, 4),

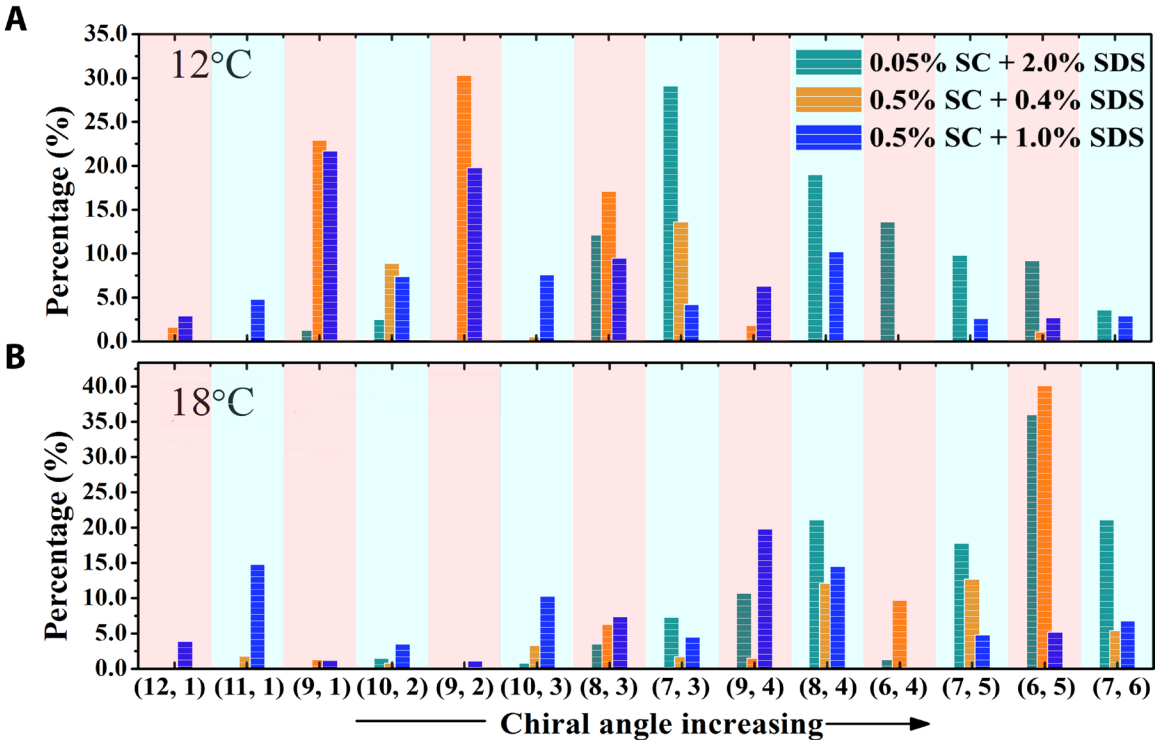


**Fig. 6. Effect of the SDS and SC concentration ratio on the chirality distribution of the SWCNTs adsorbed at 12 °C and 18 °C.** Relative content of different (*n*, *m*) species adsorbed onto gel at (**A**) 12° and (**B**) 18°C. The proportion of each (*n*, *m*) species was calculated as the ratio of the $S_{11}$ peak area of (*n*, *m*) to the sum of the $S_{11}$ peak areas.

(6, 5), and (7, 5), are adsorbed at temperatures lower than 12°C in the single-surfactant SDS system (*17*).

We developed a novel and efficient method to separate SWCNTs by chiral angle, in which the highly selective adsorption of the SWCNTs with chiral angles less than 20° into a gel medium was achieved by temperature controlling the binary surfactant system of SDS and SC. On the basis of this result, we designed a two-step strategy to separate single-chirality zigzag and near-zigzag SWCNTs: The raw SWCNT mixture was first separated by diameter using stepwise elution, and subsequently, the eluted fractions with narrow diameter distributions were separated by chiral angle through temperature control. With this technique, more than 10 types of single-chirality species, including near-zigzag SWCNTs of (9, 1), (9, 2), (10, 2), and (11, 1), were separated on the submilligram scale. We further detected the temperature-driven adsorption selectivity of SC/SDS toward the chiral angle of SWCNTs using optical absorption spectra and revealed that lowering the temperature caused the adsorption of more SC/SDS cosurfactant on the SWCNTs with smaller chiral angles, which amplified the interaction difference of the SWCNTs with different chiral angles with gel and improved the separation efficiency of SWCNTs by chiral angle. Our present results lay a fundamental basis for the industrial separation of single-chirality near-zigzag SWCNTs and provide guidance for other methods, such as ATPE and DGU, to separate small–chiral angle SWCNTs. In addition, the achievement of multiple single-chirality near-zigzag SWCNTs with a broad diameter distribution by tuning the ratio of SDS/SC provides a possible pathway for the mass separation of larger-diameter single-chirality SWCNTs, which exhibit higher carrier mobility and saturation current due to the formation of ohm contact with metal electrode.

## MATERIALS AND METHODS

### Dispersion of SWCNTs

HiPco-SWCNTs were purchased from NanoIntegris (raw powder batch no. 29-037). The as-received SWCNT powder was dispersed in 100-ml aqueous solution of 1 wt % SC (99%; Sigma-Aldrich) using a homogenizer equipped with a half-inch tip at 0.38 W/ml of output power density for 5 hours (Sonifire 450D, Branson). To dissipate the heat generated during sonication, the dispersion was immersed in a water bath at 15°C. Subsequently, ultracentrifugation (S50A, Hitachi, CS150FNX) was performed on the dispersion at 210,000*g* for 30 min. Eighty percent of the supernatant was collected as the as-prepared dispersion. SDS was introduced to the dispersion by adding SDS (99%; Sigma-Aldrich) aqueous solution of various concentrations to achieve specific concentrations of SC and SDS according to the experimental conditions. Alternatively, the raw SWCNTs were directly dispersed in the aqueous solution of 0.5 wt % SDS and 0.5 wt % SC, followed by centrifugation. The supernatant was collected as parent solution for the separation of SWCNTs.

### Temperature-controlled separation in the binary surfactant (SC and SDS) system

Several columns filled with 30 ml of gel (Sephacryl S-200 HR, GE Healthcare) were prepared. The columns, surfactant solutions, and SWCNT dispersion were soaked in a bath at 12°C. Then, 5 ml of the

dispersion was applied to an equilibrated column. The adsorbed SWCNTs were eluted by 5 wt % SDS. The flow-through fraction was collected and loaded onto the next column until no SWCNTs could be adsorbed at this temperature. Then, repeated separation of the unadsorbed SWCNTs was performed as described above after increasing the temperature at a step of 2°C.

### Mass separation of single-chirality SWCNTs with different chiral angles

Two hundred milliliters of gel was packed in a column (XK 50/40, GE Healthcare). Then, the column was connected to an automated chromatography system (AVANT 150, GE Healthcare). The whole system was kept in a homemade thermostat to control the temperature. At 18° to 22°C, the SWCNT dispersion in the mixed surfactant of 0.5 wt % SC and 1 wt % SDS was loaded onto the equilibrated column. After eluting the unadsorbed SWCNTs, the mixed surfactants *X* wt % DOC/0.5 wt % SC/1 wt % SDS were loaded to stepwise elute the adsorbed SWCNTs, where *X* was increased from 0.06 to 0.2 wt % at a step of 0.01 wt %. The eluted fractions were collected and characterized by optical absorption spectra.

Single-chirality separation of small–chiral angle SWCNTs was performed by the temperature control method. The SWCNTs in each eluted fraction from the first separation were condensed by ultracentrifugation and redispersed in the cosurfactant SDS/SC. Each as-prepared SWCNT dispersion was loaded onto the gel column at a specific set temperature to selectively adsorb single-chirality SWCNTs with smaller chiral angles. Specifically, the fractions eluted by 0.06 and 0.07 wt % DOC in the first step were redispersed in 0.5 wt % SC/0.5 wt % SDS and loaded onto a column at 15° and 18°C to adsorb the (7, 3) and (9, 1) species, respectively. The flow-through fractions were redispersed in an aqueous solution of 2 wt % SDS to adsorb (6, 4) SWCNTs at 10°C and (6, 5) SWCNTs at 14°C. The fraction eluted by 0.09 wt % DOC was redispersed in 0.5 wt % SC/0.5 wt % SDS and loaded onto a column at 15°C. (10, 2) and (8, 3) SWCNTs were eluted by 2 and 5 wt % SDS, respectively. The fraction eluted by 0.11 wt % DOC was redispersed in 0.5 wt % SC/0.5 wt % SDS. (11, 0) and (12, 1) were selectively adsorbed at 16° to 18°C and 20° to 25°C, respectively. The fraction eluted by 0.10 wt % DOC was redispersed in 0.25 wt % SC/1.25 wt % SDS, and (9, 2) nanotubes were adsorbed at 15° to 18°C. (7, 6) nanotubes were extracted from the flow-through fraction at 1.5 wt % SDS and 16° to 20°C. The fraction eluted by 0.12 wt % DOC was redispersed in 0.5 wt % SC and 1.0 wt % SDS. (10, 2) nanotubes were adsorbed at 14° to 16°C. The fractions eluted by 0.13 and 0.135 wt % DOC were redispersed in 0.25 wt % SC and 1.25 wt % SDS. (11, 1) nanotubes were adsorbed at 16° to 18°C. The flow-through dispersions were then redispersed in 2 wt % SDS, and (7, 5) and (8, 4) nanotubes were extracted at 15° and 18°C, respectively. The detailed description of the methodology is presented in fig. S4.

### Optical absorption characterization

Optical absorption spectra were recorded using an ultraviolet near-IR spectrophotometer (UV-3600, Shimadzu). A temperature control module was used to cover the cuvette and was connected to a circulating-water system to control the temperature of the sample during measurement.

## SUPPLEMENTARY MATERIALS

Supplementary material for this article is available at http://advances.sciencemag.org/cgi/content/full/7/8/eabe0084/DC1

## REFERENCES AND NOTES


1. S. M. Bachilo, M. S. Strano, C. Kittrell, R. H. Hauge, R. E. Smalley, R. B. Weisman, Structure-assigned optical spectra of single-walled carbon nanotubes. *Science* **298**, 2361–2366 (2002).
2. J. A. Misewich, R. Martel, P. Avouris, J. C. Tsang, S. Heinze, J. Tersoff, Electrically induced optical emission from a carbon nanotube FET. *Science* **300**, 783–786 (2003).
3. D. Jariwala, V. K. Sangwan, L. J. Lauhon, T. J. Marks, M. C. Hersam, Carbon nanomaterials for electronics, optoelectronics, photovoltaics, and sensing. *Chem. Soc. Rev.* **42**, 2824–2860 (2013).
4. S. Jeong, D. Yang, A. G. Beyene, J. T. Del Bonis-O'Donnell, A. M. M. Gest, N. Navarro, X. Sun, M. P. Landry, High-throughput evolution of near-infrared serotonin nanosensors. *Sci. Adv.* **5**, eaay3771 (2019).
5. Y. Piao, B. Meany, L. R. Powell, N. Valley, H. Kwon, G. C. Schatz, Y. H. Wang, Brightening of carbon nanotube photoluminescence through the incorporation of $sp^3$ defects. *Nat. Chem.* **5**, 840–845 (2013).
6. L. Liu, J. Han, L. Xu, J. Zhou, C. Zhao, S. Ding, H. Shi, M. Xiao, L. Ding, Z. Ma, C. Jin, Z. Zhang, L.-M. Peng, Aligned, high-density semiconducting carbon nanotube arrays for high-performance electronics. *Science* **368**, 850–856 (2020).
7. G. J. Brady, A. J. Way, N. S. Safron, H. T. Evensen, P. Gopalan, M. S. Arnold, Quasi-ballistic carbon nanotube array transistors with current density exceeding Si and GaAs. *Sci. Adv.* **2**, e1601240 (2016).
8. Y. Yomogida, T. Tanaka, M. Zhang, M. Yudasaka, X. Wei, H. Kataura, Industrial-scale separation of high-purity single-chirality single-wall carbon nanotubes for biological imaging. *Nat. Commun.* **7**, 12056 (2016).
9. Y. Liu, J. Zhang, H. Liu, S. Wang, L.-M. Peng, Electrically driven monolithic subwavelength plasmonic interconnect circuits. *Sci. Adv.* **3**, e1701456 (2017).
10. S. Khasminskaya, F. Pyatkov, K. Słowik, S. Ferrari, O. Kahl, V. Kovalyuk, P. Rath, A. Vetter, F. Hennrich, M. M. Kappes, G. Gol'tsman, A. Korneev, C. Rockstuhl, R. Krupke, W. H. P. Pernice, Fully integrated quantum photonic circuit with an electrically driven light source. *Nat. Photonics* **10**, 727–732 (2016).
11. A. Saha, B. J. Gifford, X. He, G. Ao, M. Zheng, H. Kataura, H. Htoon, S. Kilina, S. Tretiak, S. K. Doorn, Narrow-band single-photon emission through selective aryl functionalization of zigzag carbon nanotubes. *Nat. Chem.* **10**, 1089–1095 (2018).
12. S. Zhang, L. Kang, X. Wang, L. Tong, L. Yang, Z. Wang, K. Qi, S. Deng, Q. Li, X. Bai, F. Ding, J. Zhang, Arrays of horizontal carbon nanotubes of controlled chirality grown using designed catalysts. *Nature* **543**, 234–238 (2017).
13. F. Yang, X. Wang, D. Zhang, K. Qi, J. Yang, Z. Xu, M. Li, X. Zhao, X. Bai, Y. Li, Growing zigzag (16, 0) carbon nanotubes with structure-defined catalysts. *J. Am. Chem. Soc.* **137**, 8688–8691 (2015).
14. Q. Zhao, Z. Xu, Y. Hu, F. Ding, J. Zhang, Chemical vapor deposition synthesis of near-zigzag single-walled carbon nanotubes with stable tube-catalyst interface. *Sci. Adv.* **2**, e1501729 (2016).
15. M. He, X. Wang, S. Zhang, H. Jiang, F. Cavalca, H. Cui, J. B. Wagner, T. W. Hansen, E. Kauppinen, J. Zhang, F. Ding, Growth kinetics of single-walled carbon nanotubes with a (*2n, n*) chirality selection. *Sci. Adv.* **5**, eaav9668 (2019).
16. H. Liu, D. Nishide, T. Tanaka, H. Kataura, Large-scale single-chirality separation of single-wall carbon nanotubes by simple gel chromatography. *Nat. Commun.* **2**, 309 (2011).
17. H. Liu, T. Tanaka, Y. Urabe, H. Kataura, High-efficiency single-chirality separation of carbon nanotubes using temperature-controlled gel chromatography. *Nano Lett.* **13**, 1996–2003 (2013).
18. H. Liu, T. Tanaka, H. Kataura, Optical isomer separation of single-chirality carbon nanotubes using gel column chromatography. *Nano Lett.* **14**, 6237–6243 (2014).
19. G. Ao, J. K. Streit, J. A. Fagan, M. Zheng, Differentiating left- and right-handed carbon nanotubes by DNA. *J. Am. Chem. Soc.* **138**, 16677–16685 (2016).
20. S. Ghosh, S. M. Bachillo, R. B. Weisman, Advanced sorting of single-walled carbon nanotubes by nonlinear density-gradient ultracentrifugation. *Nat. Nanotechnol.* **5**, 443–450 (2010).
21. X. Tu, S. Manohar, A. Jagota, M. Zheng, DNA sequence motifs for structure-specific recognition and separation of carbon nanotubes. *Nature* **460**, 250–253 (2009).
22. A. Nish, J.-Y. Hwang, J. Doig, R. J. Nicholas, Highly selective dispersion of single-walled carbon nanotubes using aromatic polymers. *Nat. Nanotechnol.* **2**, 640–646 (2007).
23. F. Yang, M. Wang, D. Zhang, J. Yang, M. Zheng, Y. Li, Chirality pure carbon nanotubes: Growth, sorting, and characterization. *Chem. Rev.* **120**, 2693–2758 (2020).
24. F. Ding, A. R. Harutyunyan, B. I. Yakobson, Dislocation theory of chirality-controlled nanotube growth. *Proc. Natl. Acad. Sci. U.S.A.* **106**, 2506–2509 (2009).
25. Q. Yuan, F. Ding, How a zigzag carbon nanotube grows. *Angew. Chem. Int. Ed.* **54**, 5924–5928 (2015).
26. R. Rao, D. Liptak, T. Cherukuri, B. I. Yakobson, B. Maruyama, *In situ* evidence for chirality-dependent growth rates of individual carbon nanotubes. *Nat. Mater.* **11**, 213–216 (2012).

27. V. I. Artyukhov, E. S. Penev, B. I. Yakobson, Why nanotubes grow chiral. *Nat. Common.* **5**, 4892 (2014).
28. X. Wei, T. Tanaka, Y. Yomogida, N. Sato, R. Saito, H. Kataura, Experimental determination of excitonic band structures of single-walled carbon nanotubes using circular dichroism spectra. *Nat. Commun.* **7**, 12899 (2016).
29. X. Zeng, D. Yang, H. Liu, N. Zhou, Y. Wang, W. Zhou, S. Xie, H. Kataura, Detecting and tuning the interaction between surfactants and carbon nanotubes for their high-efficiency structure separation. *Adv. Mater. Interfaces* **5**, 1700727 (2018).
30. B. S. Flavel, M. M. Kappes, R. Kruple, F. Hennrich, Separation of single-walled carbon nanotubes by 1-dodecanol-mediated size-exclusion chromatography. *ACS Nano* **7**, 3557–3564 (2013).
31. D. Yang, J. Hu, H. Liu, S. Li, W. Su, Q. Li, N. Zhou, Y. Wang, W. Zhou, S. Xie, H. Kataura, Structure sorting of large-diameter carbon nanotubes by NaOH tuning the interactions between nanotubes and gel. *Adv. Funct. Mater.* **27**, 1700278 (2017).
32. X. Zeng, J. Hu, X. Zhang, N. Zhou, W. Zhou, H. Liu, S. Xie, Ethanol-assisted gel chromatography for single-chirality separation of carbon nanotubes. *Nanoscale* **7**, 16273–16281 (2015).
33. A. Hirano, T. Tanaka, Y. Urabe, H. Kataura, pH- and solute-dependent adsorption of single-wall carbon nanotubes onto hydrogels: Mechanistic insights into the metal/semiconducting separation. *ACS Nano* **7**, 10285–10295 (2013).
34. H. Gui, J. K. Streit, J. A. Fagan, A. R. Hight Walker, C. Zhou, M. Zheng, Redox sorting of carbon nanotubes. *Nano Lett.* **15**, 1642–1646 (2015).
35. N. K. Subbaiyan, S. Cambré, A. N. G. Parra-Vasquez, E. H. Hároz, S. K. Doorn, J. G. Duque, Role of surfactants and salt in aqueous two-phase separation of carbon nanotubes toward simple chirality isolation. *ACS Nano* **8**, 1619–1628 (2014).
36. H. Li, G. Gordeev, O. Garrity, N. A. Peyyety, P. B. Selvasundaram, S. Dehm, R. Krupke, S. Cambré, W. Wenseleers, S. Reich, M. Zheng, J. A. Fagan, B. S. Flavel, Separation of specific single-enantiomer single-wall carbon nanotubes in the large-diameter regime. *ACS Nano* **14**, 948–963 (2020).
37. H. Li, G. Gordeev, O. Garrity, S. Reich, B. S. Flavel, Separation of small-diameter single-walled carbon nanotubes in one to three steps with aqueous two-phase extraction. *ACS Nano* **13**, 2567–2578 (2019).
38. J. A. Fagan, C. Y. Khripin, C. A. S. Batista, J. R. Simpson, E. H. Hároz, A. R. H. Walker, M. Zheng, Isolation of specific small-diameter single-wall carbon nanotube species via aqueous two-phase extraction. *Adv. Mater.* **26**, 2800–2804 (2014).
39. T. P. Tyler, T. A. Shatry, B. J. Leever, M. C. Hersam, Narrow diameter distributions of metallic arc discharge single-walled carbon nanotubes via dual-iteration density gradient ultracentrifugation. *Adv. Mater.* **24**, 4765–4768 (2012).
40. R. B. Weisman, S. M. Bachilo, Dependence of optical transition energies on structure for single-walled carbon nanotubes in aqueous suspension: An empirical Kataura plot. *Nano Lett.* **3**, 1235–1238 (2003).
41. X. Wei, T. Tanaka, S. Li, M. Tsuzuki, G. Wang, Z. Yao, L. Li, Y. Yomogida, A. Hirano, H. Liu, H. Kataura, Photoluminescence quantum yield of single-wall carbon nanotubes corrected for the photon reabsorption effect. *Nano Lett.* **20**, 410–417 (2020).
42. S. K. Wiedmer, M.-L. Riekkola, M. Nydén, O. Söderman, Mixed micelles of sodium dodecyl sulfate and sodium cholate: Micellar electrokinetic capillary chromatography and nuclear magnetic resonance spectroscopy. *Anal. Chem.* **69**, 1577–1584 (1997).
43. C. Vautier-Giongo, B. L. Bales, Estimate of the ionization degree of ionic micelles based on Krafft temperature mesurements. *J. Phy. Chem. B* **107**, 5398–5403 (2003).
44. H. Sugioka, K. Matsuoka, Y. Moroi, Temperature effect on formation of sodium cholate micelles. *J. Colloid Interface Sci.* **259**, 156–162 (2003).
45. M. Rohlfing, Redshift of excitons in carbon nanotubes caused by the environment polarizability. *Phy. Rev. Lett.* **108**, 087402 (2012).
46. A. R. T. Nugraha, R. Saito, K. Sato, P. T. Araujo, A. Jorio, M. S. Dresselhaus, Dielectric constant model for environmental effects on the exciton energies of single wall carbon nanotubes. *Appl. Phys. Lett.* **97**, 091905 (2010).
47. J. G. Park, J. Smithyman, C.-Y. Lin, A. Cooke, A. W. Kismarahardja, S. Li, R. Liang, J. S. Brooks, C. Zhang, B. Wang, Effects of surfactants and alignment on the physical properties of single-walled carbon nanotubes buckpaper. *J. Appl. Phys.* **106**, 104310 (2009).
48. L.-J. Li, R. J. Nicholas, C.-Y. Chen, R. C. Darton, S. C. Baker, Comparative study of photoluminescemce of single-walled carbon nanotubes wrapping with sodium dodecyl sulfate, surfactin and polyvinylpyrrolidone. *Nanotechnology* **16**, S202–S205 (2005).
49. J. L. Blackburn, T. J. McDonald, W. K. Metzger, C. Engtrakul, G. Rumbles, M. J. Heben, Protonation effects on the branching ratio in photoexcited single-walled carbon nanotube dispersions. *Nano Lett.* **8**, 1047–1054 (2008).
50. Y. Zhao, J. G. Clar, L. Li, J. Xu, T. Yuan, J.-C. J. Bonzongo, K. J. Ziegler, Selective desorption of high-purity (6, 5) SWCNTs from hydrogels through surfactant modulation. *Chem. Commun.* **52**, 2928–2931 (2016).
51. M. Park, J. Park, J. Lee, S.-Y. Ju, Scaling of binding affinities and cooperativities of surfactants on carbon nanotubes. *Carbon* **139**, 427–436 (2018).
52. R. M. Jain, M. Ben-Naim, M. P. Landry, M. S. Strano, Competitive binding in mixed surfactant systems for single-walled carbon nanotube separation. *J. Phys. Chem. C* **119**, 22737–22745 (2015).
53. S. Lin, D. Blankschtein, Role of the bile salt surfactant sodium cholate in enhancing the aqueous dispersion stability of single-walled carbon nanotubes: A molecular dynamics simulation study. *J. Phys. Chem. B* **114**, 15616–15625 (2010).
54. N. R. Tummala, A. Striolo, SDS surfactants on carbon nanotubes: Aggregate morphology. *ACS Nano* **3**, 595–602 (2009).
55. C. A. Silvera-Batista, D. C. Scott, S. M. McLeod, K. J. Ziegler, A mechanistic study of the selective retention of SDS-suspended single-wall carbon nanotubes on agarose gels. *J. Phys. Chem. C* **115**, 9361–9369 (2011).
56. G. Bai, J. Sheng, Y. Wang, H. Wu, Y. Zhao, K. Zhuo, M. Bastos, Interaction between a hydrophobic rigid face and a flexible alkyl tail: Thermodynamics of self-assembling of sodium cholate and SDS. *J. Chem. Thermodyn.* **100**, 131–139 (2016).
57. B. Jójárt, M. Poša, B. Fiser, M. Szőri, Z. Farkaš, B. Viskolcz, Mixed micelles of sodium cholate and sodium dodecylsulphate 1:1 binary mixture at different temperatures-experimental and theoretical investigations. *PLOS ONE* **9**, e102114 (2014).
58. T. A. Shastry, A. J. Morris-Cohen, E. A. Weiss, M. C. Hersam, Probing carbon nanotube-surfactant interactions with two-dimensional DOSY NMR. *J. Am. Chem. Soc.* **135**, 6750–6753 (2013).
59. C.-J. Shih, S. Lin, M. S. Strano, D. Blankschtein, Understanding the stabilization of single-walled carbon nanotubes and graphene in ionic surfactant aqueous solutions: Large-scale coarse-grained molecular dynamics simulation-assisited DLVD theory. *J. Phys. Chem. C* **119**, 1047–1060 (2015).
60. S. Attal, R. Thiruvengadathan, O. Regev, Determination of the concentration of single-walled carbon nanotubes in aqueous dispersions using UV-visible adsorption spectroscopy. *Anal. Chem.* **78**, 8098–8104 (2006).



**Acknowledgments**

**Funding:** This work was financially supported by the National Key Research and Development Program of China (grant nos. 2020YFA0714700 and 2018YFA0208402), the National Natural Science Foundation of China (grant nos. 51820105002, 11634014, and 51872320), the Strategic Priority Research Program of Chinese Academy of Sciences (grant no. XDB33030100), the Key Research Program of Frontier Sciences, CAS (grant no. QYZDBSSW-SYS028), and the Youth Innovation Promotion Association of CAS (grant no. 2020005). **Author contributions:** H.L. proposed and supervised the project. D.Y. and H.L. designed the experiment. D.Y. performed most of experiments. L.L. performed the partial separation experiment with assistance from X.W. Y.W. and W.Z. provided technical support on PL and Raman characterization. S.X. and H.K. provided important suggestions. D.Y. and H.L. cowrote the manuscript. All authors analyzed and discussed the experimental data. **Competing interests:** D.Y., H.L., W.Z., and S.X. are inventors on a pending patent related to this work filed by China National Intellectual Property Administration (application number: 201811503891.7, 22 June 2020). The other authors declare that they have no other competing interests. **Data and materials availability:** All data needed to evaluate the conclusions in the paper are present in the paper and/or the Supplementary Materials. Additional data related to this paper may be requested from the authors.

Submitted 25 July 2020
Accepted 31 December 2020
Published 17 February 2021
10.1126/sciadv.abe0084

**Citation:** D. Yang, L. Li, X. Wei, Y. Wang, W. Zhou, H. Kataura, S. Xie, H. Liu, Submilligram-scale separation of near-zigzag single-chirality carbon nanotubes by temperature controlling a binary surfactant system. *Sci. Adv.* **7**, eabe0084 (2021).

Science Advances

# Submilligram-scale separation of near-zigzag single-chirality carbon nanotubes by temperature controlling a binary surfactant system

Dehua Yang, Linhai Li, Xiaojun Wei, Yanchun Wang, Weiya Zhou, Hiromichi Kataura, Sishen Xie and Huaping Liu

*Sci Adv* **7** (8), eabe0084.
DOI: 10.1126/sciadv.abe0084